

A meta-analysis of molecular spectroscopy databases, and prospects of molecule detection with some future facilities

Xin Liu^{1,2}, Fujun Du^{1,2}

¹ Purple Mountain Observatory, Chinese Academy of Sciences, Nanjing 210023, China;
fjdu@pmo.ac.cn

² School of Astronomy and Space Science, University of Science and Technology of China, Hefei 230026, China

Received 20XX Month Day; accepted 20XX Month Day

Abstract Molecules reside broadly in the interstellar space and can be detected via spectroscopic observations. To date, more than 271 molecular species have been identified in interstellar medium or circumstellar envelopes. Molecular spectroscopic parameters measured in laboratory make the identification of new species and derivation of physical parameters possible. These spectroscopic parameters are systematically collected into databases, two of the most commonly used being the CDMS and JPL databases. While new spectroscopic parameters are continuously measured/calculated and added to those databases, at any point in time it is the existing spectroscopic data that ultimately limits what molecules can possibly be identified in astronomical data. In this work, we conduct a meta-analysis of the CDMS and JPL databases. We show the statistics of transition frequencies and their uncertainties in these two databases, and discuss the line confusion problem under certain physical environments. We then assess the prospects of detecting molecules in common ISM environments using a few facilities that are expected to be conducting spectroscopic observations in the future. Results show that CSST/HSTDM and SKA1-mid have the potential to detect some complex organic molecules, or even amino acids, with reasonable assumptions about ISM environments.

Key words: catalogs — molecular data — ISM: molecules

1 INTRODUCTION

The interstellar gases, including those in atomic, molecular, and ionized forms, account for $\sim 99\%$ of the mass of interstellar medium (ISM), with the rest being interstellar dust. Various molecules exist in the ISM, some of which become the tracers to study the formation of stars (Shu et al. 1987) and planets (Adachi et al. 1976; Mizuno 1980). Spectral lines of these molecules can be used to derive the gas temperature, velocity, column density, and internal dynamics. Therefore, interstellar molecular spectroscopy have become one of the most commonly used diagnostic tools for ISM.

The first interstellar molecule, CH, was reported to exist through observation of absorption feature in the optical band (McKellar 1940). After the advent of radio astronomy, many more molecular species were detected thanks to the increasing sensitivity and spatial/spectral resolution of facilities. As of 2021, 241¹ (McGuire 2022) molecular species consisting of 18 elements were reported to exist in ISM or

¹ At the time of writing, the number of interstellar molecules included in CDMS is 271 (<https://cdms.astro.uni-koeln.de/classic/molecules>).

circumstellar envelopes (CSE) (including unconfirmed ones). These molecules are made up of 2–70 atoms, and their transition frequencies range from microwave to ultraviolet bands (McGuire 2022).

The identification of interstellar molecules, in essence, is to infer the abundances of different molecules and physical parameters of interstellar gas. Technically, this is an optimization problem. It tries to find the best set of parameters with regard to some optimization goal, which is usually the difference between the simulated and observed spectrum. In the case of a positive identification, the individual lines in simulated spectrum is supposed to match those in observation with the right line widths and intensities (Belloche et al. 2008). The simulated spectrum is calculated using the radiative transfer equation and usually (but not always) under the assumption of local thermodynamic equilibrium (LTE). As key parameters in the radiative transfer equation, molecular spectroscopy data are the foundation of the molecule identification process.

Databases such as the one maintained by Jet Propulsion Laboratory² (JPL), the Cologne Database for Molecular Spectroscopy³ (CDMS), the High-resolution TRANsmission molecular absorption database⁴ (HITRAN), and the NIST Atomic Spectra Database⁵ provide spectroscopy data to simulate spectral lines. Among these databases, JPL and CDMS are frequently used by radio astronomers in molecular identification. In this paper we present a meta-analysis of the JPL and CDMS spectroscopic databases.

A meta-analysis of these two databases can tell us which species have the potential to be detected at present and which transition lines are more likely to be resolved under certain astrophysical environments. We can estimate the integration time needed for a certain facility to detect the spectral lines of any molecular species with given astrophysical parameters. In general, a meta-analysis of current molecular databases may provide useful insights for future molecular identification. In Section 2 we present a brief description of radiative transfer, followed up with the meta-analysis of molecular spectroscopy databases in Section 3. We discuss what molecules can be observed and how much time it will cost to observe certain molecular species in Section 4, followed by a conclusion in Section 5.

2 RADIATIVE TRANSFER

About 90 percent molecules are detected in radio frequency range (McGuire 2022). This is mainly because of the composition of molecules and the environment where they reside in: the low temperature of molecular clouds means that the electronic and vibrational emissions of molecules cannot occur (absorption of background sources do sometimes occur); the large moment of inertia of these molecules (except for molecular hydrogen) lead to small rotational constants thus low transition frequencies.

The interactions of radiation field with matter can be expressed by the radiative transfer equation (Rybicki & Lightman 1979) as

$$\frac{dI_\nu}{ds} = -\alpha_\nu I_\nu + j_\nu, \quad (1)$$

where α_ν and j_ν are the absorption and emission coefficient, respectively, I_ν the specific intensity, s the travel path. This equation can be integrated as

$$I(\nu) = I_0(\nu)e^{-\tau_\nu} + S_\nu(T)(1 - e^{-\tau_\nu}). \quad (2)$$

Here S_ν is referred to as the source function, which in LTE assumption equals the Planck blackbody radiation function B_ν of the same temperature. $I_0(\nu)$ is the background radiation, T the excitation temperature, and τ the optical depth which is defined as the integration of α_ν along the travel path s :

$$\tau_\nu = \int \alpha_\nu ds = \frac{c^2}{8\pi\nu_0^2} \frac{g_u e^{-E_l/kT}}{Q(T)} N_{\text{tot}} A_{ul} [1 - e^{-h\nu_0/kT}] \varphi(\nu), \quad (3)$$

² <https://spec.jpl.nasa.gov/ftp/pub/catalog/catdir.html>

³ <https://cdms.astro.uni-koeln.de/classic/entries/>

⁴ <https://hitran.org>

⁵ <https://physics.nist.gov/PhysRefData/ASD>

where T is assumed to be independent of s , c the speed of light, ν_0 the transition frequency, g_u the statistical weight of the u energy level, E_l the energy of l level, $Q(T)$ the partition function, N_{tot} the total column density, A_{ul} the Einstein A coefficient, h the Planck constant, k the Boltzmann constant, and $\varphi(\nu)$ the line profile function. The Einstein A_{ul} coefficient describes the probability per unit time of a molecule in an excited energy level E_u to return spontaneously to a lower energy level E_l (Wilson et al. 2009). A_{ul} is related with the other two Einstein coefficients B_{ul} and B_{lu} via

$$A_{ul} = \frac{8\pi h\nu_0^3}{c^3} B_{ul}, \quad (4)$$

$$g_l B_{lu} = g_u B_{ul}. \quad (5)$$

in which g_l is the statistical weight of the l energy level. Molecular spectroscopy data, including $Q(T)$, g_u , E_l , A_{ul} , and ν_0 , are needed when calculating the spectral line intensity, which can be accessed through several databases.

3 A META-ANALYSIS OF MOLECULAR SPECTROSCOPY DATABASES

3.1 The CDMS and JPL spectroscopic databases

The JPL provides spectroscopy data “based on the project needs of astronomers” (Pickett et al. 1998) and CDMS catalogs “molecules that are present or are supposed to be present in ISM or CSE or in planetary atmospheres” (Müller et al. 2001). CDMS/JPL provides spectroscopic data for 1137/401 species, of which 189 are available in both databases. Each line of a data file contains the frequency ν and its uncertainty, the base 10 logarithm of integrated intensity I at 300 K, degree of freedom in the rotational partition function, lower state energy E_l , upper state degeneracy g_u , and the quantum numbers. These data can be accessed through their websites and downloaded in ASCII format. The Einstein A coefficient can be calculated as (Pickett et al. 1998):

$$A_{ul} = I(300\text{ K})\nu^2 \frac{Q(T)}{g_u(e^{-E_l/kT} - e^{-E_u/kT})} \times 2.7964 \times 10^{-16} \quad (6)$$

where E_u is the upper state energy. CDMS provides an interface to search for all transitions within a given frequency range, and plot their intensities as a function of frequency under some simple assumptions online (Müller et al. 2005).

Regarding the 189 species that are included in both the CDMS and JPL databases, their entries can be classified into four cases. Some of them contain completely identical transitions except for the precision of spectroscopy data. The transitions of several species in one database are the subsets of those in another. Some pairs have a part of identical transitions (again, except for the precision) and additional unique ones in each database. The rest pairs are complementary to each other, with no repeating transition.

CDMS also participates in the Virtual Atomic and Molecular Data Centre and provides data in MySQL database format⁶ (Endres et al. 2016). Different from the files directly downloaded from their website, this database file contains the Einstein A coefficients rather than the integrated intensity. Molecular species in JPL are also included in this database file.

3.2 Transition Frequency Distribution

The transition frequencies range from 0.4 kHz to $\sim 166,000$ GHz in CDMS and 0.4 kHz to ~ 857845 GHz in JPL. In Fig. 1 we show the histogram of transition frequencies of all the species in CDMS and JPL in a log–log scale. The number of transitions in each 10,000 km/s velocity interval rises from ~ 10 at ~ 0.01 MHz to $\sim 100,000$ at ~ 1000 GHz and then decreases sharply. Quantitatively, about 99%, 90%, and 50% of these frequencies fall in the intervals from 8 to 21,420 GHz, 70 to 3098 GHz,

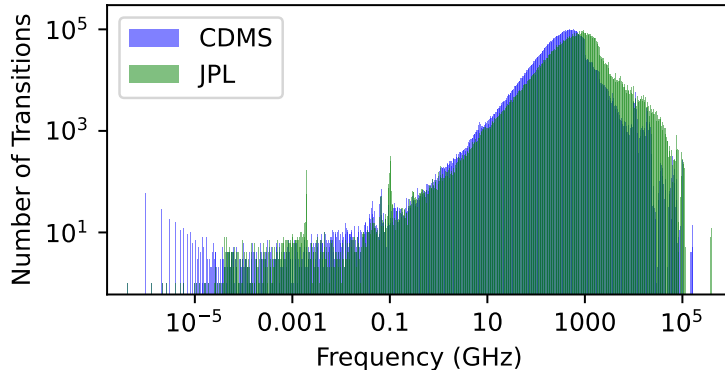


Fig. 1: Histograms of the transition frequencies of molecules in CDMS and JPL. Each bin represents the velocity width of 10,000 km/s. Data from CDMS are in purple and JPL in light green.

and 266 to 985 GHz, respectively. Nearly two hundred of transitions have extremely low frequencies ($< 10^{-5}$ GHz), which are all from the rotational transitions of CH_3OH , $\text{CH}_3^{18}\text{OH}$, and H_2CO . These three asymmetric top molecules are close to symmetric top structures, so the extremely low energy difference between two energy levels, which is caused by the deviation from the symmetric top case, leads to extremely low transition frequencies. They are calculated in theory but may not be detectable in practice because of the extremely low frequency and intensity.

3.3 Frequency Uncertainty

Molecular spectroscopy data are either calculated theoretically or measured in laboratory, and the precision of these data determines the reliability of molecular identification. Files provided by CDMS and JPL include the uncertainty of transition frequencies, which ranges from 0–1 GHz. This frequency error can be translated into a velocity error as

$$v_{\text{err}} = \frac{\nu_{\text{err}}}{\nu} \cdot c, \quad (7)$$

where ν is the transition frequency and ν_{err} represents its uncertainty. Figure 2 gives the distribution of frequency uncertainties and velocity errors of all transitions in both CDMS and JPL. Most of these uncertainties are low enough that the majority of velocity errors are under 1 km/s.

The internal turbulent motion of gas flows make their radial velocities have a finite velocity width. Assuming a typical velocity width $\Delta v \lesssim 10$ km/s (FWHM), if the velocity error of a transition is comparable to or greater than the velocity width, it is difficult to attribute the spectral line to its corresponding molecule. For this reasons, we divided all velocity errors into three levels, $v_{\text{err}} < 1$ km/s, $1 \text{ km/s} \leq v_{\text{err}} < 10$ km/s, and $v_{\text{err}} \geq 10$ km/s, as reliable, suspicious, and unreliable, respectively. We assigned the three levels with different colors and drew a velocity error distribution map in Fig. 3, where we can see that except for those calculated theoretically (uncertainty= 0 MHz), spectroscopy data with frequencies lower than 0.1 GHz are less reliable than those with higher frequencies, and data with higher intensities are also more reliable. All data with relatively low frequencies ($\nu < 0.1$ GHz) and low intensity ($\lg I_\nu < -25 \text{ nm}^2 \cdot \text{MHz}$) have high velocity errors ($v_{\text{err}} > 10$ km/s), and they are all from the isotopomers of either O_2 or OH. The relatively large pie charts are in the 100–1000 GHz range, which means more transitions are cataloged in this frequency range. In general, most of these transitions are reliable.

⁶ http://cdms.ph1.uni-koeln.de/cdms/portal/cdms_lite.db.gz

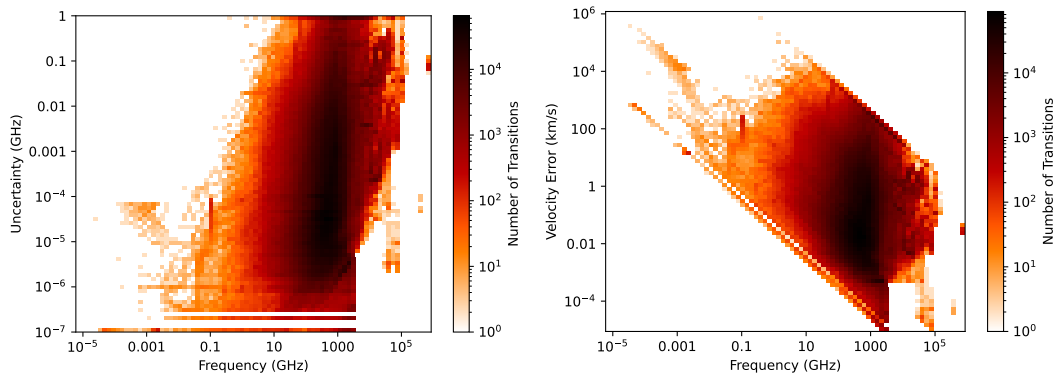


Fig. 2: 2D histogram of frequency uncertainties and the corresponding velocity errors in both CDMS and JPL.

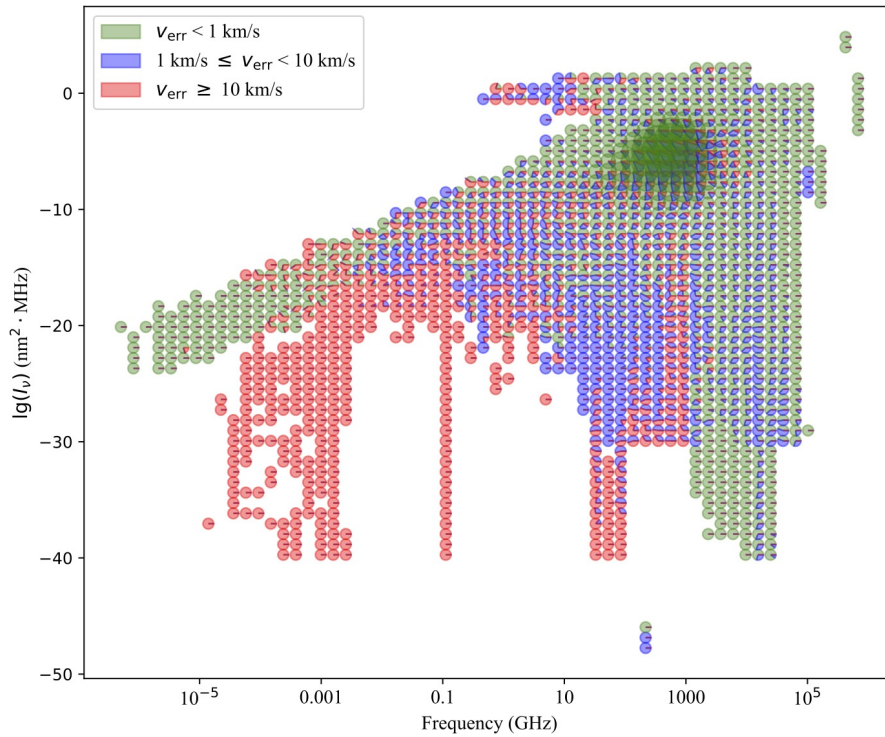


Fig. 3: The distribution of velocity errors in a frequency-intensity map. Each pie chart was filled with at most three colors: green, purple, and red, corresponding to fractions of frequencies that are reliable, tentative, and unreliable, respectively. A bigger pie chart means a greater number of transition lines are cataloged in this frequency-intensity range.

3.4 Line Confusion

If two transition lines have similar intensities, and the separation of line centers is less than either of their line widths, these two lines are considered to be blended, which is known as the line confusion problem. To discuss this issue, we assume that all previously identified molecules are present in an

interstellar cloud, and have a constant excitation temperature of 20 K and an FWHM velocity width of 5 km/s. The column densities are set to their typical values that obtained from literature⁷. Those without definite literature values are all belong to vibrational/electronic excited states or minor isotopomers. For the latter ones we adopt empirical isotope ratios of H/D = 1000 (Persson et al. 2013), $^{12}\text{C}/^{13}\text{C} = 59$, $^{14}\text{N}/^{15}\text{N} = 237$, $^{32}\text{S}/^{34}\text{S} = 19$ (Lucas & Liszt 1998), $^{16}\text{O}/^{18}\text{O} = 672$ (Wilson et al. 1981), $^{16}\text{O}/^{17}\text{O} = 1935$ (Wouterloot et al. 2008), $^{28}\text{Si}/^{29}\text{Si} = 13$, $^{28}\text{Si}/^{30}\text{Si} = 12$ (Wolff 1980), and $^{35}\text{Cl}/^{37}\text{Cl} = 2.1$ (De Luca et al. 2012) to derive rough column density values from their main isotopomer instead, while those in vibrational/electronic excited states are not included for the lack of good estimations of their column densities. We must note that the H/D ratio varies dramatically under the influence of difference chemical processes in low temperature, and a reasonable mean value of 1000 is adopted here. We then define the line confusion as the number of spectral lines in each 10 km/s interval in the simulated spectrum, and arbitrarily call intervals with more than five transitions as “crowded”. Lines with extremely low intensities ($T_{\text{mb}} < 0.01$ K) are not included for line-confusion counting.

Figure 4 shows the number of crowded intervals in each 1 GHz bin from 0 to 2000 GHz, from

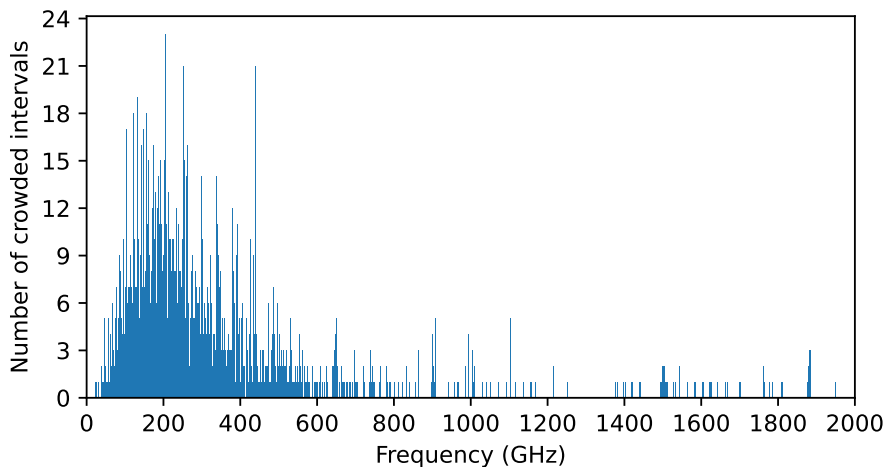


Fig. 4: The distribution of “crowded” intervals which is defined in Section 3.4. Each bin represents a frequency width of 1 GHz.

which we know that transitions between ~ 50 and 600 GHz are more crowded than those in higher or low frequency ranges. Note that all previously detected molecules are included to give an overview of the line confusion, but this may oversimplify the reality. A source is unlikely to have all these molecules, and the excitation conditions of molecules may differ from one to another. Some sources contain multiple velocity components, which may aggravate the problem of line confusion.

4 SUGGESTIONS FOR FUTURE OBSERVATIONS

For a given source, we would like to know which transitions can be obtained at certain noise level using a given telescope within a reasonable integration time, and we also want to figure out how much time it would take if we intend to search for certain molecular species, or what physical environment should this molecule reside in if it is detectable.

With regard to these concerns, we investigate the observability of molecules using a few major facilities that would be operating in the future. To calculate the line intensities, we consider three types of ISM environments: i) a cold diffuse source with an angular size (θ_s) of $60''$ and an excitation temperature

⁷ These values and corresponding references are available on Github: https://github.com/LiuXnhhh/paper_materials

(T_{ex}) of 10 K (Pratap et al. 1997); ii) a hot dense core with an angular size of $3''$ and an excitation temperature of 200 K (Belloche et al. 2013); iii) an intermediate case with an angular size of $40''$ and an excitation temperature of 30 K. These three cases are summarized in Table 1. Column densities are set

Table 1: Three sets of assumed physical parameters for simulating molecular spectra.

	T_{ex} (K)	θ_s ($''$)
Case 1	10	60
Case 2	200	3
Case 3	30	40

to their typical measured values, as mentioned in Section 3.4. A typical line width of 5 km/s is assumed for all lines. The beam filling factor for a source s is defined as

$$\eta_s = \frac{\theta_s^2}{\theta_s^2 + \theta_t^2}, \quad (8)$$

where θ_t is the half-power beamwidth of a telescope. This factor becomes important when the source is not extended. The cosmic microwave background (CMB) radiation ($T_{\text{CMB}} = 2.725$ K) is also considered. Lines with the peak intensities higher than three times sensitivity (σ) are taken as detectable, and molecular species with more than three detectable transitions are regarded as unambiguous identifications (Snyder et al. 2005). Molecular spectroscopy data used in this section are mainly taken from CDMS and is supplemented by those in JPL. Note that the column densities of nearly one third of molecules are derived from empirical isotope ratios. These molecules are either minor isotopomers or in a vibrational/electronic excited state thus may be less abundant than assumed, causing the overestimation of their line intensities. Thus the detectabilities stated here can only be viewed as an optimistic estimation, and is valid only for molecules under LTE conditions. To ensure the reliability of the predictions, we have compared the synthesized spectra with the line survey reported by Belloche et al. (2013) using the same physical parameters. Results show that our simulated lines are almost identical to their synthetic spectra. We will benchmark the performance of current spectral line modeling programs and discuss this in future.

4.1 The Terahertz module of CSST

The high-sensitivity terahertz detection module (HSTDM) (Zhang et al. 2018) onboard Chinese Space Station Telescope (CSST) covers a frequency range of 410–510 GHz. CSST has a diameter of 2 m, which means at the working band of HSTDM the beamwidth is $\sim 70''$. With a frequency resolution of 0.1 MHz, the receiver promises to be able to reach a 3σ noise level of 0.15 K with 200 s of integration.

4.1.1 Molecules that are observable in one hour

Among all previously identified molecules and their isotopomers, 25/21/58 of them can be detected by CSST/HSTDM within one hour in case 1/2/3, respectively (see Tables 2, 3, and 4). We take two molecules of special significance or with relatively more detectable transitions as examples and discuss their observability in detail.

CH_3OH and $^{13}\text{CH}_3\text{OH}$ In case 1/2/3, 48/60/135 transition lines of CH_3OH and 98/322/265 lines of $^{13}\text{CH}_3\text{OH}$ can be detected within one hour. As one of the most prominent molecules expected to be detected by CSST/HSTDM, several transitions of $^{13}\text{CH}_3\text{OH}$ in 234–238 GHz (Sutton et al. 1985) and 488 to 571 GHz (Persson et al. 2007) have already been detected in different lines of sight. Interstellar CH_3OH , the main isotopomer of $^{13}\text{CH}_3\text{OH}$, can be used to trace the interface between outflows and ambient gas (Plambeck & Menten 1990) and compact H II regions (Batra et al. 1987), and is thought to

Table 2: List of potentially detectable molecules with one hour of integration by CSST/HSTDM in case 1.

2 Atoms	3 Atoms	4 Atoms	5 Atoms	6 Atoms	8 Atoms	9 Atoms
CN	C ₂ H	DNCO	CH ₂ NH	¹³ CH ₃ OH	H ₂ NCONH ₂	CH ₃ CH ₂ CN
NO	DCO ⁺	H ₂ CO	HCOCN	CH ₃ OH		¹³ CH ₃ CH ₂ CN
	H ₂ Cl ⁺	HONO	HNCNH	H ₂ CCNH		CH ₃ ¹³ CH ₂ CN
	NH ₂	NH ₂ D				C ₂ H ₅ ¹³ CN
	SO ₂					CH ₃ OCH ₃
	Si ₂ C					
	TiO ₂					

Table 3: List of potentially detectable molecules with one hour of integration by CSST/HSTDM in case 2.

2 Atoms	3 Atoms	5 Atoms	6 Atoms	8 Atoms	9 Atoms	> 9 Atoms
AlO	AlOH	HC ₃ N	¹³ CH ₃ OH	H ₂ NCONH ₂	CH ₃ CH ₂ CN	CH ₃ OCH ₂ OH
CN	DCO ⁺		CH ₃ OH	NH ₂ CH ₂ CN	¹³ CH ₃ CH ₂ CN	<i>i</i> -C ₃ H ₇ CN
PO	SO ₂		H ₂ CCNH		CH ₃ ¹³ CH ₂ CN	
TiO	TiO ₂				C ₂ H ₅ ¹³ CN	
					C ₂ H ₅ C ¹⁵ N	

Notes: The descriptor "*i*-" (*iso*) of C₃H₇CN means the four C atoms form a branched skeleton.

Table 4: List of potentially detectable molecules with one hour of integration by CSST/HSTDM in case 3.

2 Atoms	3 Atoms	4 Atoms	5 Atoms	6 Atoms	7 Atoms	8 Atoms	9 Atoms	> 9 Atoms
AlF	AlOH	DNCO	CH ₃ Cl	¹³ CH ₃ OH	<i>c</i> -C ₂ H ₄ O	CH ₂ OHCHO	¹³ CH ₃ ¹³ CH ₂ CN	CH ₃ CH ₂ OCHO
AlO	C ₂ H	H ¹³ CO*	CH ₃ ³⁷ Cl	CH ₃ OH	<i>s</i> -H ₂ CCHOH	H ₂ NCONH ₂	¹³ CH ₃ CH ¹³ CN	CH ₃ OCH ₂ OH
¹³ CN	DCO ⁺	H ₂ CO	H ₂ CNH	H ₂ CCNH		NH ₂ CH ₂ CN	¹³ CH ₃ CH ₂ CN	<i>aGg'</i> -(CH ₂ OH) ₂
CN	H ₂ Cl ⁺	HNCO	HCOCN				C ₂ H ₅ ¹³ CN	<i>gGg'</i> -(CH ₂ OH) ₂
FeO	HNO	HONO	HNCNH				C ₂ H ₅ C ¹⁵ N	<i>i</i> -C ₃ H ₇ CN
NO	NH ₂	NH ₂ D					CH ₂ DCH ₂ CN*	<i>n</i> -C ₃ H ₇ CN
NS	SO ₂						CH ₃ ¹³ CH ¹³ CN	
PO	Si ₂ C						CH ₃ ¹³ CH ₂ CN	
SO	TiO ₂						CH ₃ CH ₂ CN	
SiC							CH ₃ CH ₂ OH	
SiN							CH ₃ CHDCN*	
TiO							CH ₃ OCH ₃	

Notes: *Molecules with column densities derived from their main isotopomer. The descriptor "*c*-" in *c*-C₂H₄O represents the O atom and two C atoms that are arranged in a *cyclic* form. The "*s*-" in *s*-H₂CCHOH means the "*syn*-" form of the molecule, with the H atom in hydroxyl and CH₂ radical on the same side of the C—O bond. The "*aGg'*-" and "*gGg'*-" represent two rotational isomers of (CH₂OH)₂: *G* (*gauche*) means two hydroxymethyls are ±60° apart, and *a* (*anti*), *g*, *g'* mean the hydroxyl and hydroxymethyl are 180°, 60°, and -60° apart, respectively. The "*n*-" (*normal*) means the four C atoms in C₃H₇CN are arranged in a straight chain.

be related to the formation of complex organic molecules (Öberg et al. 2009). Since both ¹³CH₃OH and CH₃OH can be detected by CSST/HSTDM in all three cases, one can use them to derive the ¹³C/¹²C ratio.

We have considered three assumed cases to give an overview of which molecules can be detected, but they may not be the environments where CH₃OH and ¹³CH₃OH reside in. More realistically, we revisit the spectral lines of ¹³CH₃OH and CH₃OH which reside in Orion-KL with an angular size of 12'' (Schilke et al. 2001) and different excitation temperatures. Results show that they both can be detected when the excitation temperature is higher than ~12 K.

CN The high frequency resolution of CSST/HSTDM enables the detection of CN and its hyper-fine components at ~ 453 GHz. The Zeeman effect of CN can be used as a direct measurement of strengths of magnetic fields (Crutcher et al. 1996) and has already been detected toward a few dense clouds through its $N = 1 \rightarrow 0$ transition at ~ 113 GHz (Crutcher et al. 1999). The CN $N = 4 \rightarrow 3$ transition (452–454 GHz) has 19 hyper-fine components, of which six have relatively strong intensities. We adopt an average angular size of $58''$ (Savage et al. 2002) for several galactic molecular clouds, and find that these six lines are detectable from $T_{\text{ex}} \simeq 8$ K all along to ~ 300 K. But according to the project plan of CSST/HSTDM, polarization capability for measuring magnetic field with the Zeeman effect is not implemented.

4.1.2 Prebiotic molecules

Prebiotic molecules are those “that are thought to be involved in the processes leading to the origin of life” (Herbst & van Dishoeck 2009). Amino acids, the basic building blocks of living creatures, are one of the prebiotic molecules most searched for by astronomers. Kvenvolden et al. (1970) discovered five abundant amino acids in meteorites, and now more than 80 species of amino acids were detected in meteorites (Cronin & Pizzarello 1997; Koga & Naraoka 2017, etc.). While no spectral line of interstellar amino acids has been unambiguously confirmed, their possible precursors such as formic acid (HCOOH) (Zuckerman et al. 1971), amino acetonitrile ($\text{NH}_2\text{CH}_2\text{CN}$) (Belloche et al. 2008), and isocyanic acid (HNCO) (Snyder & Buhl 1972) have been detected. We carried out several simulations on observing prebiotic molecules to investigate how long it would take if we would like to detect them in different astrophysical environments.

Glycine As the simplest amino acid, glycine ($\text{H}_2\text{NCH}_2\text{COOH}$) can form on the analogous of interstellar grains (Bernstein et al. 2002). Several attempts (Cunningham et al. 2007; Jones et al. 2007) had been made to search for its lowest energy conformer I and higher energy conformer II, but failed. In the consideration of an unambiguous identification, we choose three brightest lines of glycine conformer I (hereafter glycine, for convenience) to investigate their detectability under a wider range of ($T_{\text{ex}}, N_{\text{tot}}$) combinations. The difference between three cases in Table 1 thus only lies in the source sizes, which behave as the dilution factor of line intensities. To avoid redundancy, we only discuss the detectability of glycine under case 3 (hereafter for all prebiotic molecule discussions). For each line we draw a detectability plot in Fig. 5, where the integration time requirement for detecting glycine under a certain combination of ($T_{\text{ex}}, N_{\text{tot}}$) can be figured out. Jones et al. (2007) assumed an excitation temperature of 75 K and derived an upper limit of $1.4 \times 10^{15} \text{ cm}^{-2}$ for the column density for extend ($\eta = 1$) glycine in an eight-hour observation. As a comparison, assuming the same excitation temperature, CSST/HSTDM could possibly detect glycine with a column density of $\sim 1 \times 10^{15} \text{ cm}^{-2}$ in 10 hr even though a smaller beam filling factor ($\eta \simeq 0.23$) is adopted. However, we must note that the actual column density of interstellar glycine (if it exists) could be much lower than the value we assumed here.

Alanine Same as glycine, alanine ($\text{CH}_3\text{CHNH}_2\text{COOH}$) is also able to form on the analogous of interstellar grains and has two conformers. More importantly, it is one of the only two amino acids (besides glycine) included in CDMS. The detectability of alanine is shown in Fig. 6. Compared with those of glycine, the spectral lines of alanine is fainter thus more difficult to be detected with CSST/HSTDM.

c-HCOOH ⁸ According to Cuadrado et al. (2016), c-HCOOH is thought to be formed via fluorescent decay from excited t-HCOOH in ultraviolet irradiated gas, making c-HCOOH not only a related species of amino acids but a tracer of photodissociation regions. Limited by its low column density, this molecule was only detected using the line stacking analysis and $T_{\text{ex}} \simeq 21$ K and $N_{\text{tot}} \simeq 4 \times 10^{12} \text{ cm}^{-2}$ was derived (Cuadrado et al. 2016). We can tell from Fig. 7 that CSST/HSTDM could detect c-HCOOH with the same temperature and column density in about 20 hr using regular methods.

⁸ The descriptor “c-” represent the two H atoms are on the same side of C-O single bond.

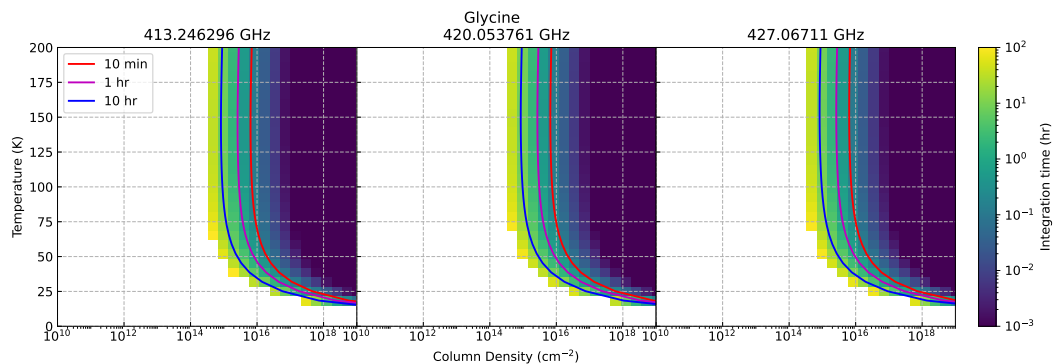


Fig. 5: Integration time requirement for CSST/HSTDM to observe three different transitions of glycine. Each pixel in the figure represents a $(T_{\text{ex}}, N_{\text{tot}})$ combination, while the color scale indicates the integration time needed for a 3σ detection, with more than 100 hours set to white. Red, magenta, and blue contours mark out $(T_{\text{ex}}, N_{\text{tot}})$ combinations required for each transition to be detected with an integration time of 10 minutes, 1 hour, and 10 hours, respectively.

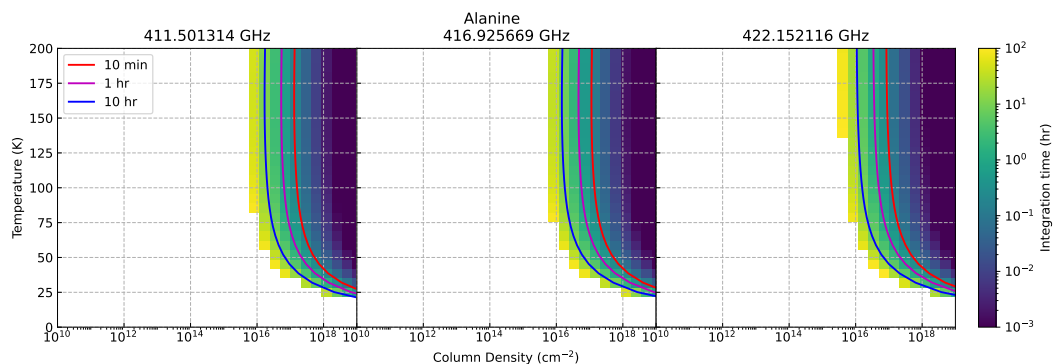


Fig. 6: Integration time requirement for CSST/HSTDM to observe three transitions of alanine.

As to the line confusion problem, if all previously identified molecules are present as we assumed, lines of these prebiotic molecules may be blended by those of others. More explicitly, among above-mentioned strong lines, the 413.246296 GHz line of glycine is slightly blended by previously identified molecules; all three c-HCOOH lines are blended, but its several weaker lines around 455 and 509 GHz are free from confusion.

4.2 SKA-mid

The mid-frequency range (0.58–25 GHz) of the initial phase of Square Kilometer Array (hereafter SKA1-mid) will consist of 133 15 m SKA1 dishes and 64 13.5 m MeerKAT telescopes⁹. By means of interferometry, SKA1-mid can reach a high angular resolution ($\eta \simeq 1$). Taking advantages of the frequency resolution (13.44 kHz) and sensitivity (a system temperature of ~ 33 K at 10 GHz), SKA1-mid can be used to search for amino acids and other prebiotic molecules (Carilli & Rawlings 2004).

⁹ https://www.skatelescope.org/wp-content/uploads/2021/02/22380.Construction-Proposal_DIGITAL_v3.pdf

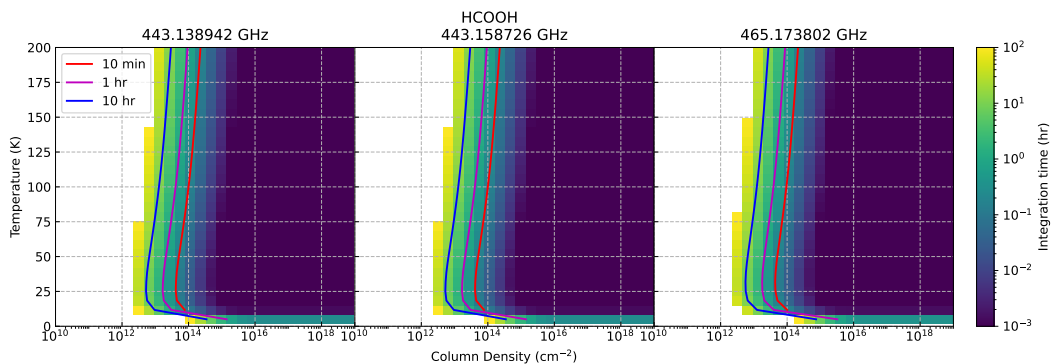


Fig. 7: Integration time requirement for CSST/HSTDM to observe three transitions of *c*-HCOOH.

4.2.1 Molecules that are observable in one hour

Because of the higher mass and larger sizes, more complex molecules have larger moment of inertia. The same quantized angular momentum corresponds to lower energy levels. Compared with CSST/HSTDM, SKA1-mid covers a lower frequency range, making it more capable of detecting complex molecules. As shown in Table 5, 6, and 7, more complex molecules, especially carbon chain molecules (C_nH , $HC_{2n+1}N$, etc.), are detectable in one hour under all three cases.

Table 5: List of potentially detectable molecules with one hour of integration by SKA1-mid in case 1.

2 Atoms	3 Atoms	4 Atoms	5 Atoms	6 Atoms	7 Atoms	8 Atoms	9 Atoms	> 9 Atoms
OH	MgNC NaCN	C ₃ S DNCO	C ₄ H HCOCN	C ₅ H C ₅ N ⁻	¹³ CH ₃ OH MgC ₅ N <i>c</i> -C ₂ H ₄ O	¹³ CH ₂ OHCHO* CH ₂ OH ¹³ CHO* CH ₂ OHCHO H ₂ C ₆ H ₂ NCONH ₂ NH ₂ CH ₂ CN	¹³ CH ₃ ¹³ CH ₂ CN ¹³ CH ₃ CH ₂ ¹³ CN ¹³ CH ₃ CH ₂ CN C ₂ H ₅ ¹³ CN C ₂ H ₅ C ¹⁵ N C ₈ H CH ₂ D ^{oop} CH ₂ CN* CH ₃ ¹³ CH ₂ ¹³ CN CH ₃ ¹³ CH ₂ CN CH ₃ CH ₂ CN CH ₃ CH ₂ OH CH ₃ CH ₂ SH CH ₃ CHDCN* CH ₃ OCH ₃ HC ₇ N	C ₂ H ₅ NCO CH ₃ CH ₂ OCHO CH ₃ OCH ₂ OH <i>aGg'</i> -(CH ₂ OH) ₂ <i>gGg'</i> -(CH ₂ OH) ₂ <i>i</i> -C ₃ H ₇ CN <i>n</i> -C ₃ H ₇ CN <i>s</i> -C ₂ H ₅ CHO

Notes: The superscript “^{oop}” in CH₂D^{oop}CH₂CN means the D atom are out of the C_S plane. The prefix “*s*-” of C₂H₅CHO represents the formyl and methyl are 0° apart from each other.

Table 6: List of potentially detectable molecules with one hour of integration by SKA1-mid in case 2.

2 Atoms	3 Atoms	4 Atoms	6 Atoms	7 Atoms	8 Atoms	9 Atoms	> 9 Atoms
OH	SO ₂ TiO ₂	¹⁵ NH ₃ NH ₂ D NH ₃	¹³ CH ₃ OH CH ₃ OH H ₂ CCNH	HC ₅ N	CH ₂ OHCHO H ₂ NCONH ₂ NH ₂ CH ₂ CN	¹³ CH ₃ ¹³ CH ₂ CN ¹³ CH ₃ CH ₂ ¹³ CN ¹³ CH ₃ CH ₂ CN C ₂ H ₅ ¹³ CN C ₂ H ₅ C ¹⁵ N CH ₂ D ^{oop} CH ₂ CN* CH ₃ ¹³ CH ₂ ¹³ CN CH ₃ ¹³ CH ₂ CN CH ₃ CH ₂ CN CH ₃ CHDCN*	CH ₃ CH ₂ OCHO CH ₃ OCH ₂ OH <i>aGg'</i> -(CH ₂ OH) ₂ <i>gGg'</i> -(CH ₂ OH) ₂ <i>i</i> -C ₃ H ₇ CN <i>n</i> -C ₃ H ₇ CN

Table 7: List of potentially detectable molecules with one hour of integration by SKA1-mid in Case 3.

2 Atoms	3 Atoms	4 Atoms	5 Atoms	6 Atoms	7 Atoms	8 Atoms	9 Atoms	> 9 Atoms
OH	SO ₂	HONO	C ₄ H	¹³ CH ₃ OH	HC ₅ N	CH ₂ OHCHO	¹³ CH ₃ ¹³ CH ₂ CN	CH ₃ CH ₂ OCHO
	Si ₂ C	¹⁵ NH ₃	HCOCN	CH ₃ OH	<i>c</i> -C ₂ H ₄ O	H ₂ C ₆	¹³ CH ₃ CH ₂ ¹³ CN	CH ₃ OCH ₂ OH
	TiO ₂	NH ₂ D	SiC ₄	H ₂ CCNH		H ₂ NCONH ₂	¹³ CH ₃ CH ₂ CN	<i>aGg'</i> -(CH ₂ OH) ₂
		NH ₃				NH ₂ CH ₂ CN	C ₂ H ₅ ¹³ CN	<i>gGg'</i> -(CH ₂ OH) ₂
							C ₂ H ₅ C ¹⁵ N	<i>i</i> -C ₃ H ₇ CN
							CH ₂ D ^{o,p} CH ₂ CN*	<i>n</i> -C ₃ H ₇ CN
							CH ₃ ¹³ CH ₂ ¹³ CN	
							CH ₃ ¹³ CH ₂ CN	
							CH ₃ CH ₂ CN	
							CH ₃ CH ₂ SH	
							CH ₃ CHDCN*	
							CH ₃ OCH ₃	
							HC ₇ N	

HC_{2n+1}N Such carbon chain molecules are generally abundant in early stage dense molecular cores before carbon atoms become locked in CO (Sakai & Yamamoto 2013). Therefore, they can be used as tracers of dark clouds and starless cores. The case 1 have a similar physical environment with TMC-1, where HC₅N, HC₇N, HC₉N, and HC₁₁N have already been detected (Avery et al. 1976; Broten et al. 1978; Kroto et al. 1978; Loomis et al. 2021). Towards the same source, SKA1-mid can detect HC₅N within 5 seconds, HC₇N in 10 minutes, and HC₉N in 4 hr. Loomis et al. (2021) derived an excitation temperature of 6.6 K and a velocity width of 0.117 km/s for HC₁₁N using line stacking techniques. We use the same parameters as them and find that three brightest HC₁₁N lines can be individually detected by SKA1-mid without stacking in 10 minutes.

4.2.2 Prebiotic molecules

Glycine and alanine In Fig. 8 we present the detectability of glycine and alanine using SKA1-mid. If the typical temperature of a cold dense molecular cloud is set to ~ 35 K (Brown et al. 1979), glycine molecules with column densities of $\sim 1 \times 10^{15} \text{ cm}^{-2}$ can be detected in 10 hr. The same holds for alanine.

Ethanolamine As the simplest phospholipid head group, ethanolamine (NH₂CH₂CH₂OH) has been identified by Rivilla et al. (2021) with $T_{\text{ex}} \simeq 10$ K and $N_{\text{tot}} \simeq 1.5 \times 10^{13} \text{ cm}^{-2}$. For the same excitation temperature and column density SKA1-mid can detect it within 30 hr, as seen in Fig. 9.

Amino acetonitrile As a possible direct precursor of glycine, amino acetonitrile (H₂NCH₂CN) is thought to be abundant in ISM (Pizzarello & Huang 2005), and has already been identified by Belloche et al. (2008) with $T_{\text{ex}} \simeq 100$ K and $N_{\text{tot}} \simeq 2.8 \times 10^{16} \text{ cm}^{-2}$. We present the detectability of H₂NCH₂CN in Fig. 10. It shows that SKA1-mid can detect H₂NCH₂CN in 10 hr even if the column density is two orders of magnitude lower.

The working band of SKA1-mid is less crowded than that of CSST/HSTDM, making these prebiotic molecules more possible to be unambiguously identified. More than ten strong lines of glycine and alanine are unblended or only weakly blended by those of previously identified molecules. Although the three strongest amino acetonitrile lines present in Fig. 10 are all weakly blended, several weaker lines are free from line confusion.

4.3 FAST

Compared with two telescopes mentioned above, the Five-hundred-meter Aperture Spherical radio Telescope (FAST) at present covers a narrower frequency range from 1.05 to 1.45 GHz, and has a frequency resolution of ~ 0.48 kHz. The beamwidth decreases from $\sim 251''$ at 1 GHz to $140''$ at 1.8 GHz

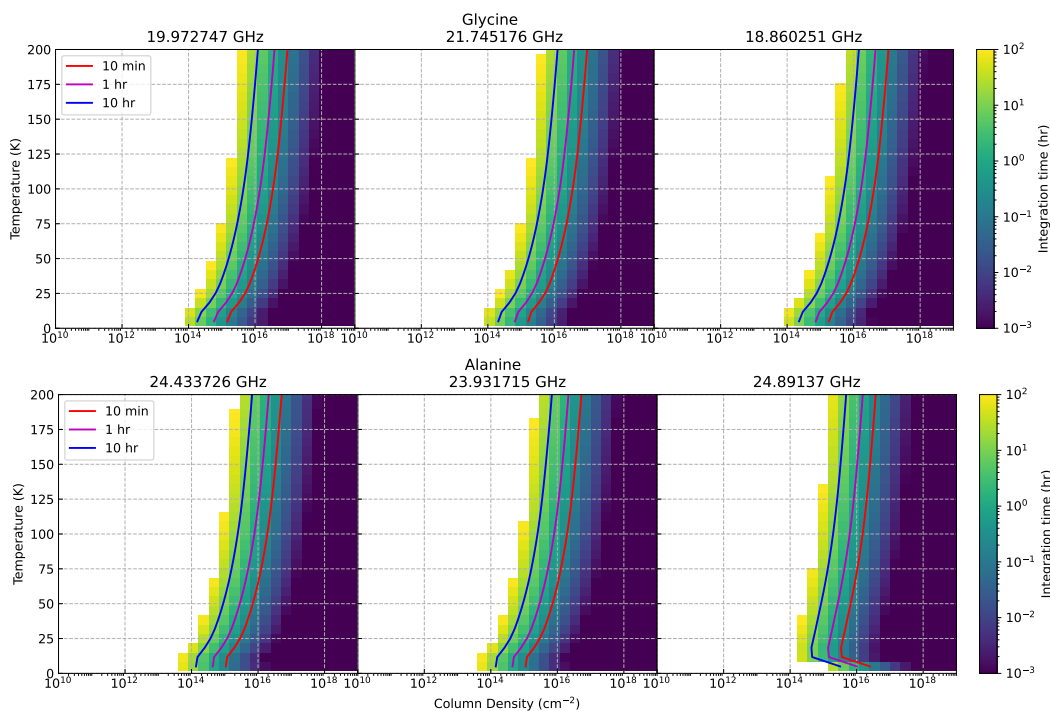


Fig. 8: Integration time requirement for SKA1-mid to observe three transitions of glycine (*top*) and alanine (*bottom*).

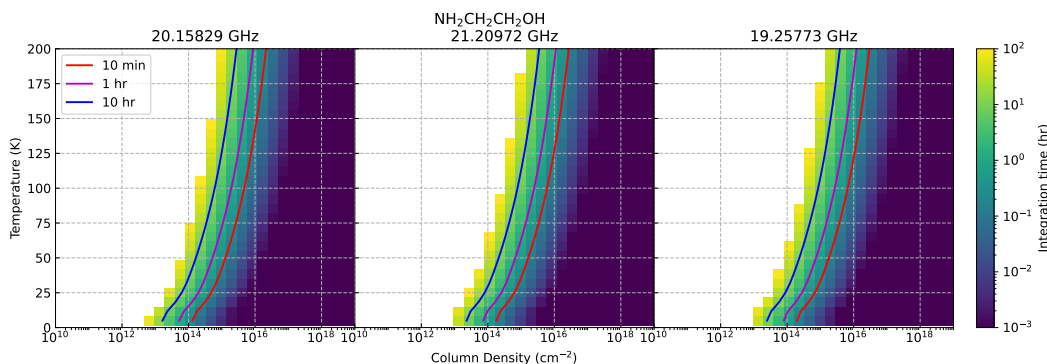


Fig. 9: Integration time requirement for SKA1-mid to observe three transitions of NH₂CH₂CH₂OH.

with a diameter of 300 m. For simplicity we adopt a constant system temperature of 24 K (Jiang et al. 2020), yielding a 3σ noise level of ~ 2.32 K at 1.4 GHz in 1 second. Limited by the frequency coverage, only ¹³CH₃OH in cases 3 can be detected by FAST within one hour.

If the frequency coverage can slightly extend to a higher range, the OH molecule can be detected by FAST via its four ground state lines: ²Π_{3/2} (J=3/2) at 1665.4018 (F=1-1), 1667.3590 (F=2-2), 1612.2310 (F=1-2), and 1720.5300 MHz (F=2-1). The maser emission of the ~ 1665 and 1667 MHz lines are associated with star-forming and their ambient ultracompact H II regions (Caswell 1998); the 1612 MHz maser line is used to trace the shell structure of evolved stars (Hyland et al. 1972); the 1720 MHz maser line is known to be a probe of shocks (Lockett et al. 1999). All these four OH maser

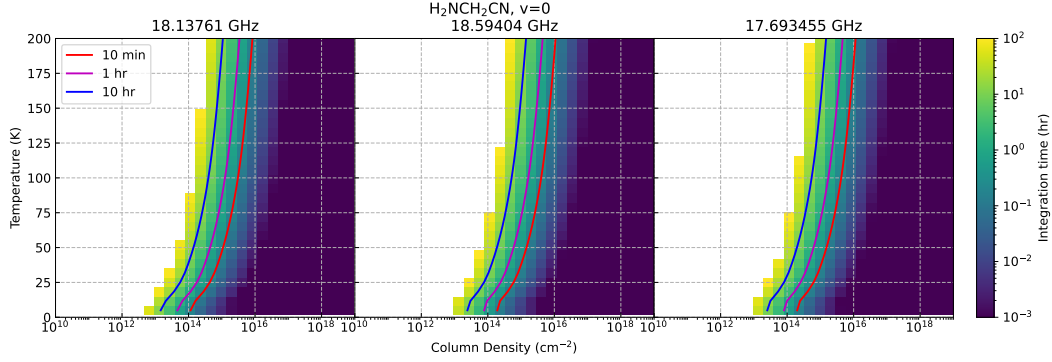


Fig. 10: Integration time requirement for SKA1-mid to observe three transitions of $\text{H}_2\text{NCH}_2\text{CN}$.

lines have been detected by Arecibo telescope (Lewis 1997; Kanekar et al. 2018). Using the same facility, Troland & Crutcher (2008) conducted ~ 500 hr of OH Zeeman observations to derive the magnetic field of nine dark cloud cores, and McBride & Heiles (2013) measured the Zeeman effect of two main maser lines (1665 and 1669 MHz). As the largest single-aperture telescope, FAST should be able to detect these four lines as well as their possible maser emission and Zeeman effect.

However, our estimation shows that no prebiotic molecules can be unambiguously detected by FAST within 100 hr with its current receiver system.

4.4 Detection by absorption in the presence of a background continuum source

Since many complex organic molecules were detected in massive star-forming regions (Belloche et al. 2013), we calculate the spectral lines of prebiotic molecules that are present in front of a bright source, as sketched in Fig. 11. The background source is taken to be a blackbody.

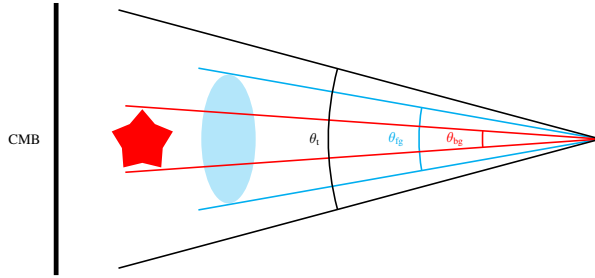


Fig. 11: A sketch of molecular gas (cyan) in front of a background continuum source (red) and CMB (black). Here θ_{bg} , θ_{fg} , θ_{t} represent the angular sizes of background, foreground, and telescope, respectively.

Equation 2, taking CMB and filling factors into consideration, can be rewritten as:

$$I(\nu) = [\eta_{\text{fg}} S_{\nu}(T_{\text{fg}}) - \eta_{\text{fg}} S_{\nu}(T_{\text{CMB}}) - \eta_{\text{bg}} B_{\nu}(T_{\text{bg}})](1 - e^{-\tau_{\nu}}), \quad (9)$$

where T_{bg} represents the temperature of background source, η_{fg} and η_{bg} the filling factors of foreground molecules and the background source, respectively. The $I(\nu)$ here represents the intensity difference between transition lines and the background continuum (i.e. the spectral baseline has been subtracted), one thus may obtain a negative spectral line intensity, i. e. absorption line, if the $\eta_{\text{bg}} B_{\nu}(T_{\text{bg}})$ term exceeds the first two terms. Absorption lines with the minimum intensities 3σ lower than the local continuum are taken as detectable. Parameters in cases 1, 2, and 3 remain unaltered except for a background source

with a temperature of 200 K and an angular size (θ_{bg}) of 0.''5, which resembles a hot core in Sagittarius B2 molecular cloud (Bonfand et al. 2017).

The extremely small η_{bg} for CSST/HSTDM ($\sim 10^{-5}$) and FAST ($\sim 10^{-6}$) make the spectra almost identical to those with no background source, namely, no absorption feature can be observed with the parameter set assumed here. For SKA1-mid, we continue to assume $\eta_{bg} = 1$ thus a brightness temperature of 200 K for the background continuum. That is to say, in case 2 of Table 1, when the excitation temperature of the foreground source is around 200 K, the small difference between the background and foreground temperature will lead to a low line intensity thus requires a large amount of integration time. For this reason, only NH_3 , $\text{CH}_3\text{CH}_2\text{CN}$, $^{13}\text{CH}_3\text{OH}$, $i\text{-C}_3\text{H}_7\text{CN}$, $^{15}\text{NH}_3$, OH, $\text{C}_2\text{H}_5^{13}\text{CN}$, and $\text{CH}_3^{13}\text{CH}_2\text{CN}$ can be detected by SKA1-mid within one hour in this case. Detectable molecules under cases 1 and 3 within one hour using SKA1-mid are listed in Tables 8 and 9, respectively. Many more molecules can be detected in case 1 and 3 when introducing the background source.

Table 8: List of potentially detectable molecules in front of a bright source with one hour of integration by SKA1-mid in case 1.

2 Atoms	3 Atoms	4 Atoms	5 Atoms	6 Atoms	7 Atoms	8 Atoms	9 Atoms	> 9 Atoms
CH	C_2S	C_3N	C_4H	$^{13}\text{CH}_3\text{OH}$	C_6H	$^{13}\text{CH}_2\text{OHCHO}^*$	$^{13}\text{CH}_3^{13}\text{CH}_2\text{CN}$	$\text{C}_2\text{H}_5\text{NCO}$
KCl	CaNC	C_3S	CH_2CN	C_5H	C_6H^-	C_7H	$^{13}\text{CH}_3\text{CH}_2^{13}\text{CN}$	$\text{C}_2\text{H}_5\text{NH}_2$
OH	KNC	C_3^3S^*	H_2CCO	C_5N^-	CH_2CHCN	$\text{CH}_2\text{ODCHO}^*$	$^{13}\text{CH}_3\text{CH}_2\text{CN}$	$\text{CH}_3\text{C}_5\text{N}$
SiH	MgNC	DNCO	H_2NCN	C_5S	CH_3NCO , $\nu_b=0$	$\text{CH}_2\text{OH}^{13}\text{CHO}^*$	$\text{C}_2\text{H}_5^{13}\text{CN}$	$\text{CH}_3\text{CH}_2\text{OCHO}$
	NaCN	H_2CS	HCOCN	CH_3OH	$\text{H}^{13}\text{CC}_4\text{N}^*$	$\text{CH}_2\text{OHCHO}^*$	$\text{C}_2\text{H}_5\text{C}^{15}\text{N}$	$\text{CH}_3\text{CH}_3\text{CO}$
	SO_2	$\text{HN}^{13}\text{CO}^*$	HCCNC	CH_3SH	$\text{HC}^{13}_2\text{CC}_2\text{N}^*$	CH_2CCHCN	C_8H	$\text{CH}_3\text{CHCH}_2\text{O}$
	Si_2C	HONO	HNCCC	$E\text{-HNCHCN}$	$\text{HC}^{13}_3\text{CCN}^*$	CH_2CHCHO	$\text{CH}_2\text{D}^{\text{opp}}\text{CH}_2\text{CN}^*$	$\text{CH}_3\text{OCH}_2\text{OH}$
	SiC_2	HSCN	MgC_3N	H_2CCNH	$\text{HC}^{13}_4\text{CN}^*$	CH_2OHCHO	$\text{CH}_3^{13}\text{CH}_2^{13}\text{CN}$	HC_{11}N
	TiO_2	$^{15}\text{NH}_3$	SiC_4	MgC_4H	HC_4NC	$\text{CH}_3\text{C}_3\text{N}$	$\text{CH}_3^{13}\text{CH}_2\text{CN}$	HC_9N
		NH_3	$c\text{-HCOOH}$	SiH_3CN	HC_5N	CH_3COOH , $\nu_t=0$	$\text{CH}_3\text{C}_4\text{H}$	$\text{NH}_2\text{CH}_2\text{CH}_2\text{OH}$
		$c\text{-C}_3\text{H}$	$t\text{-HCOSH}$	$Z\text{-HNCHCN}$	HC_5^*O	CHDOHCHO^*	$\text{CH}_3\text{CH}_2\text{CN}$	$aGg'-(\text{CH}_2\text{OH})_2$
				$L\text{-C}_4\text{H}_2$	HC_5O	H_2C_6	$\text{CH}_3\text{CH}_2\text{OH}$	$gGg'-(\text{CH}_2\text{OH})_2$
				$L\text{-HC}_4\text{N}$	$\text{HC}^{13}\text{CC}_3\text{N}^*$	H_2NCONH_2	$\text{CH}_3\text{CH}_2\text{SH}$	$i\text{-C}_3\text{H}_7\text{CN}$
					HOCH_2CN	HC_5NH^+	$\text{CH}_3\text{CHDCN}^*$	$n\text{-C}_3\text{H}_7\text{CN}$
					MgC_5N	MgC_6H	CH_3OCH_3	$s\text{-C}_2\text{H}_5\text{CHO}$
					$c\text{-C}_2\text{H}_4\text{O}$	$\text{NH}_2\text{CH}_2\text{CN}$	DC_7N	
					$s\text{-H}_2\text{CCHOH}$		HC_7^*N	
							HC_7N	

Notes: The prefix “L-” of C_4H_2 and HC_4N mean the C atoms are arranged in a *linear* form, while the “c-” in front of C_3H describe a *cyclic* form. The “t-” prefix of HCOSH represents the two H atoms are on the opposite side of the C-S bond. *E*- and *Z*- HNCHCN describe the H atom and cyanyl on the same and opposite side, respectively.

Table 9: List of potentially detectable molecules in front of a bright source with one hour of integration by SKA1-mid in case 3.

2 Atoms	3 Atoms	4 Atoms	5 Atoms	6 Atoms	7 Atoms	8 Atoms	9 Atoms	> 9 Atoms
KCl	C_2S	C_3S	C_4H	$^{13}\text{CH}_3\text{OH}$	CH_2CHCN	$^{13}\text{CH}_2\text{OHCHO}^*$	$^{13}\text{CH}_3^{13}\text{CH}_2\text{CN}$	$\text{C}_2\text{H}_5\text{NCO}$
OH	MgNC	DNCO	H_2CCO	C_5H	$\text{H}^{13}\text{CC}_4\text{N}^*$	$\text{CH}_2\text{OH}^{13}\text{CHO}^*$	$^{13}\text{CH}_3\text{CH}_2^{13}\text{CN}$	$\text{CH}_3\text{CH}_2\text{OCHO}$
	NaCN	H_2CO	H_2CNH	C_5N^-	$\text{HC}^{13}_2\text{CC}_2\text{N}^*$	CH_2OHCHO	$^{13}\text{CH}_3\text{CH}_2\text{CN}$	$\text{CH}_3\text{CH}_3\text{CO}$
	SO_2	HONO	H_2NCN	C_5S	$\text{HC}^{13}_3\text{CCN}^*$	$\text{CH}_3\text{C}_3\text{N}$	$\text{C}_2\text{H}_5^{13}\text{CN}$	$\text{CH}_3\text{OCH}_2\text{OH}$
	Si_2C	HSCN	HCOCN	CH_3OH	$\text{HC}^{13}_4\text{CN}^*$	CH_3COOH , $\nu_t=0$	$\text{C}_2\text{H}_5\text{C}^{15}\text{N}$	HC_9N
	SiC_2	$^{15}\text{NH}_3$	MgC_3N	H_2CCNH	HC_5N	H_2C_6	C_8H	$aGg'-(\text{CH}_2\text{OH})_2$
	TiO_2	NH_2D	SiC_4	MgC_4H	$\text{HC}^{13}\text{CC}_3\text{N}^*$	H_2NCONH_2	$\text{CH}_2\text{D}^{\text{opp}}\text{CH}_2\text{CN}^*$	$gGg'-(\text{CH}_2\text{OH})_2$
		NH_3		$Z\text{-HNCHCN}$	MgC_5N	MgC_6H	$\text{CH}_3^{13}\text{CH}_2^{13}\text{CN}$	$i\text{-C}_3\text{H}_7\text{CN}$
				$L\text{-C}_4\text{H}_2$	$c\text{-C}_2\text{H}_4\text{O}$	$\text{NH}_2\text{CH}_2\text{CN}$	$\text{CH}_3^{13}\text{CH}_2\text{CN}$	$n\text{-C}_3\text{H}_7\text{CN}$
							$\text{CH}_3\text{CH}_2\text{CN}$	$s\text{-C}_2\text{H}_5\text{CHO}$
							$\text{CH}_3\text{CH}_2\text{OH}$	
							$\text{CH}_3\text{CH}_2\text{SH}$	
							$\text{CH}_3\text{CHDCN}^*$	
							CH_3OCH_3	
							HC_7N	

Figure 12 shows the detectability of glycine and alanine. We already discussed in Sec. 4.2.2 that glycine and alanine have the potential to be detected by SAK1-mid via their emission lines in a reasonable time. Under our assumptions, their absorption lines are even easier to detect when the excitation temperatures are low ($\lesssim 10$ K): it would take 10 hr for SKA1-mid to detect glycine/alanine even if the column density is as low as $7 \times 10^{12}/2 \times 10^{13} \text{ cm}^{-2}$.

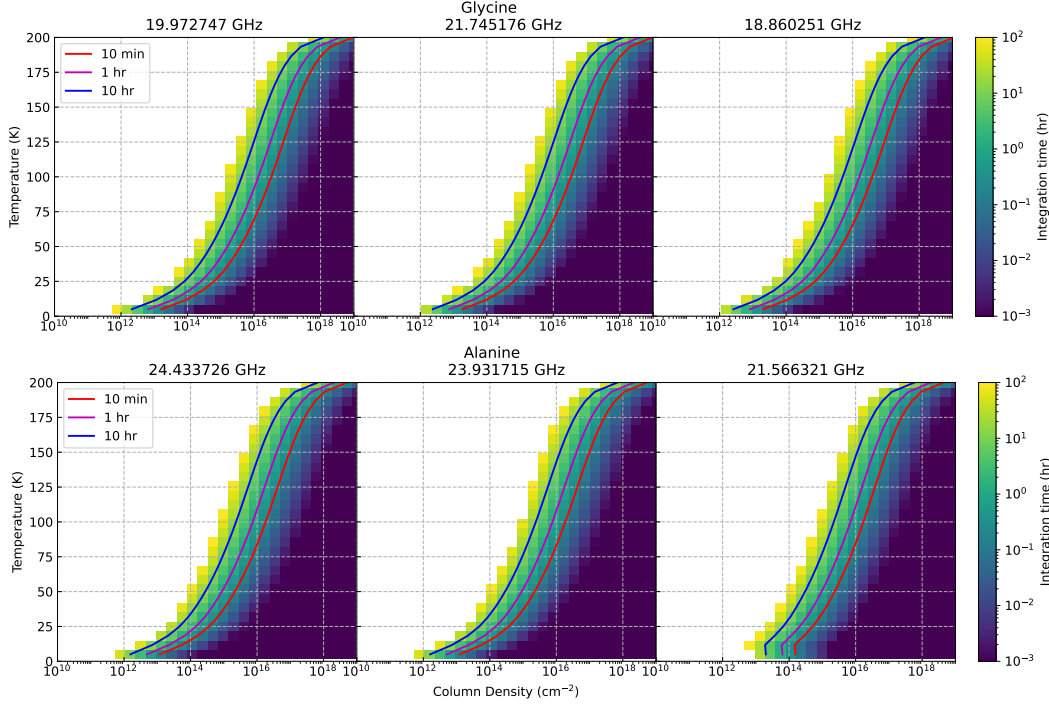


Fig. 12: Integration time requirement for SKA1-mid to observe the absorption lines of glycine (*top*) and alanine (*bottom*) for $T_{\text{bg}} = 200$ K and $\theta_{\text{bg}} = 0.5''$.

5 CONCLUSION

Molecular spectroscopic data are at the base of the molecule identification process. A meta-analysis of related databases gives us a clue about the prospects of future detection of interstellar molecules. The main results of this paper are as follows:

- 1) Most transitions in CDMS and JPL reside in 100–1000 GHz. Transitions within 10–1000 GHz mostly have low frequency uncertainties, and most transitions with high frequency uncertainties are faint (hence unimportant anyway).
- 2) Under some common assumptions, the frequency concentration between 100 and 1000 GHz makes this range more likely to suffer from line confusion problems, causing it more difficult to confirm a molecular species in this frequency range.
- 3) More simple molecules can be detected by the HSTDM onboard CSST, while SKA1-mid can detect more complex molecules with one-hour of observation in a variety of ISM environments. Due to the narrow frequency coverage by far, only OH and $^{13}\text{CH}_3\text{OH}$ can possibly be observed by FAST in one hour with plausible assumptions on their column densities.
- 4) Prebiotic molecules such as glycine with a column density of $\sim 1 \times 10^{15} \text{ cm}^{-2}$ can be detected by CSST/HSTDM in a 10 hr; SKA1-mid is able to detect glycine and alanine with $N_{\text{tot}} \gtrsim 1 \times$

10^{15} cm^{-2} and $T_{\text{ex}} \simeq 35 \text{ K}$ in 10 hr. Several strong lines of them are likely not blended by the lines of other molecules hence are ideal for the identification of these molecules.

- 5) How a bright background source influences the detectability of molecules depends on its angular size and brightness temperature. For SKA1-mid, the introduction of a bright background source behind a cold dense molecular cloud makes prebiotic molecules easier to detect via absorption features. Compared with emission, glycine/alanine with column densities as low as $7 \times 10^{12}/2 \times 10^{13} \text{ cm}^{-2}$ are able to be detected by SKA1-mid by absorption in 10 hr under our assumptions. Because of the extremely small filling factor, the compact background source has little influence on the detectability of molecules while using CSST/HSTDM and FAST.
- 6) When discussing the line confusion problem and detectable molecules in one hour, we simply set the excitation temperature and velocity width of previously identified molecules to the same typical value, respectively, and the column densities of these molecules to their literature or empirical values. These assumptions are oversimplified because the physical parameters may vary dramatically under different interstellar environments. Besides, only one velocity component is considered for each source, which surely underestimate the line confusion problem in crowded regions. When talking about the detectability of prebiotic molecules, the velocity width is fixed to a constant. In the future we will investigate ways to predict the detectability of molecules more realistically.

Acknowledgements We thank the referee for his/her constructive suggestions which help to improve the quality of the paper. This work is financially supported by the National Natural Science Foundation of China through grants 12041305 and 11873094, and by the China Manned Space Project.

References

- Adachi, I., Hayashi, C., & Nakazawa, K. 1976, *Progress of Theoretical Physics*, 56, 1756 1
- Avery, L. W., Broten, N. W., MacLeod, J. M., Oka, T., & Kroto, H. W. 1976, *ApJ*, 205, L173 12
- Batra, W., Matthews, H. E., Menten, K. M., & Walmsley, C. M. 1987, *Nature*, 326, 49 7
- Belloche, A., Menten, K. M., Comito, C., et al. 2008, *A&A*, 482, 179 2, 9, 12
- Belloche, A., Müller, H. S. P., Menten, K. M., Schilke, P., & Comito, C. 2013, *A&A*, 559, A47 7, 14
- Bernstein, M. P., Dworkin, J. P., Sandford, S. A., Cooper, G. W., & Allamandola, L. J. 2002, *Nature*, 416, 401 9
- Bonfand, M., Belloche, A., Menten, K. M., Garrod, R. T., & Müller, H. S. P. 2017, *A&A*, 604, A60 15
- Broten, N. W., Oka, T., Avery, L. W., MacLeod, J. M., & Kroto, H. W. 1978, *ApJ*, 223, L105 12
- Brown, R. D., Godfrey, P. D., Storey, J. W. V., et al. 1979, *MNRAS*, 186, 5P 12
- Carilli, C. L., & Rawlings, S. 2004, *New Astron. Rev.*, 48, 979 10
- Caswell, J. L. 1998, *MNRAS*, 297, 215 13
- Cronin, J. R., & Pizzarello, S. 1997, *Science*, 275, 951 9
- Crutcher, R. M., Troland, T. H., Lazareff, B., & Kazes, I. 1996, *ApJ*, 456, 217 9
- Crutcher, R. M., Troland, T. H., Lazareff, B., Paubert, G., & Kazès, I. 1999, *ApJ*, 514, L121 9
- Cuadrado, S., Goicoechea, J. R., Roncero, O., et al. 2016, *A&A*, 596, L1 9
- Cunningham, M. R., Jones, P. A., Godfrey, P. D., et al. 2007, *MNRAS*, 376, 1201 9
- De Luca, M., Gupta, H., Neufeld, D., et al. 2012, *ApJ*, 751, L37 6
- Endres, C. P., Schlemmer, S., Schilke, P., Stutzki, J., & Müller, H. S. 2016, *Journal of Molecular Spectroscopy*, 327, 95 3
- Herbst, E., & van Dishoeck, E. F. 2009, *ARA&A*, 47, 427 9
- Hyland, A. R., Becklin, E. E., Frogel, J. A., & Neugebauer, G. 1972, *A&A*, 16, 204 13
- Jiang, P., Tang, N.-Y., Hou, L.-G., et al. 2020, *Research in Astronomy and Astrophysics*, 20, 064 13
- Jones, P. A., Cunningham, M. R., Godfrey, P. D., & Cragg, D. M. 2007, *MNRAS*, 374, 579 9
- Kanekar, N., Ghosh, T., & Chengalur, J. N. 2018, *Phys. Rev. Lett.*, 120, 061302 14
- Koga, T., & Naraoka, H. 2017, *Scientific Reports*, 7, 636 9
- Kroto, H. W., Kirby, C., Walton, D. R. M., et al. 1978, *ApJ*, 219, L133 12
- Kvenvolden, K., Lawless, J., Pering, K., et al. 1970, *Nature*, 228, 923 9

- Lewis, B. M. 1997, *ApJS*, 109, 489 14
- Lockett, P., Gauthier, E., & Elitzur, M. 1999, *ApJ*, 511, 235 13
- Loomis, R. A., Burkhardt, A. M., Shingledecker, C. N., et al. 2021, *Nature Astronomy*, 5, 188 12
- Lucas, R., & Liszt, H. 1998, *A&A*, 337, 246 6
- McBride, J., & Heiles, C. 2013, *ApJ*, 763, 8 14
- McGuire, B. A. 2022, *ApJS*, 259, 30 1, 2
- McKellar, A. 1940, *PASP*, 52, 187 1
- Mizuno, H. 1980, *Progress of Theoretical Physics*, 64, 544 1
- Müller, H. S. P., Thorwirth, S., Roth, D. A., & Winnewisser, G. 2001, *A&A*, 370, L49 3
- Müller, H. S., Schlöder, F., Stutzki, J., & Winnewisser, G. 2005, *Journal of Molecular Structure*, 742, 215 3
- Öberg, K. I., Garrod, R. T., van Dishoeck, E. F., & Linnartz, H. 2009, *A&A*, 504, 891 8
- Persson, C. M., Olofsson, A. O. H., Koning, N., et al. 2007, *A&A*, 476, 807 7
- Persson, M. V., Jørgensen, J. K., & van Dishoeck, E. F. 2013, *A&A*, 549, L3 6
- Pickett, H. M., Poynter, R. L., Cohen, E. A., et al. 1998, *J. Quant. Spec. Radiat. Transf.*, 60, 883 3
- Pizzarello, S., & Huang, Y. 2005, *Geochim. Cosmochim. Acta*, 69, 599 12
- Plambeck, R. L., & Menten, K. M. 1990, *ApJ*, 364, 555 7
- Pratap, P., Dickens, J. E., Snell, R. L., et al. 1997, *ApJ*, 486, 862 7
- Rivilla, V. M., Jiménez-Serra, I., Martín-Pintado, J., et al. 2021, *Proceedings of the National Academy of Science*, 118, 2101314118 12
- Rybicki, G. B., & Lightman, A. P. 1979, *Radiative processes in astrophysics* 2
- Sakai, N., & Yamamoto, S. 2013, *Chemical Reviews*, 113, 8981 12
- Savage, C., Apponi, A. J., Ziurys, L. M., & Wyckoff, S. 2002, *ApJ*, 578, 211 9
- Schilke, P., Benford, D. J., Hunter, T. R., Lis, D. C., & Phillips, T. G. 2001, *The Astrophysical Journal Supplement Series*, 132, 281 8
- Shu, F. H., Adams, F. C., & Lizano, S. 1987, *ARA&A*, 25, 23 1
- Snyder, L. E., & Buhl, D. 1972, *ApJ*, 177, 619 9
- Snyder, L. E., Lovas, F. J., Hollis, J. M., et al. 2005, *ApJ*, 619, 914 7
- Sutton, E. C., Blake, G. A., Masson, C. R., & Phillips, T. G. 1985, *ApJS*, 58, 341 7
- Troland, T. H., & Crutcher, R. M. 2008, *ApJ*, 680, 457 14
- Wilson, R. W., Langer, W. D., & Goldsmith, P. F. 1981, *ApJ*, 243, L47 6
- Wilson, T. L., Rohlfs, K., & Hüttemeister, S. 2009, *Tools of Radio Astronomy* 3
- Wolff, R. S. 1980, *ApJ*, 242, 1005 6
- Wouterloot, J. G. A., Henkel, C., Brand, J., & Davis, G. R. 2008, *A&A*, 487, 237 6
- Zhang, K., Shi, S., Yao, Q., et al. 2018, in *2018 International Conference on Microwave and Millimeter Wave Technology (ICMMT)*, 1 7
- Zuckerman, B., Ball, J. A., & Gottlieb, C. A. 1971, *ApJ*, 163, L41 9